Inorg. Chem. **2003**, *42*, 7173–7181

Novel ET-Coordinated Copper(I) Complexes: Syntheses, Structures, and Physical Properties (ET = BEDT-TTF = Bis(ethylenedithio)tetrathiafulvalene)

Ryo Kanehama,[†] Masamichi Umemiya,[†] Fumiyasu Iwahori,[†] Hitoshi Miyasaka,[†] Ken-ichi Sugiura,[†] Masahiro Yamashita,*[,†] Yasukata Yokochi,[‡] Hiroshi Ito,[‡] Shin-ichi Kuroda,[‡] Hideo Kishida,[§] and Hiroshi Okamoto[§]

Department of Chemistry, Tokyo Metropolitan University and CREST, Minami-ohsawa 1-1, Hachioji 192-0397, Japan, Department of Applied Physics, Nagoya University, Nagoya 464-8603, Japan, and Graduate School of Frontier Science, University of Tokyo, Kashiwa, Chiba 277-8561, Japan

Received April 24, 2003

New molecular charge-transfer complexes of bis(ethylenedithio)tetrathiafulvalene (ET), $(ET)Cu_2Br_4$ (**1**), $(ET)_2Cu_6Br_{10}$ (**2**), $(ET)_2[Cu_4Br_6ET]$ (**3**), $(ET)_2Cu_2Br_4$ (**4**), $(ET)_2Cu_3Br_7(H_2O)$ (**5**), and $(ET)_2Cu_6Br_{10}(H_2O)_2$ (**6**), have been synthesized by diffusing reaction of ET and $Cu^{II}Br_2$. Their crystal structures and physical properties have been investigated. X-ray analyses revealed that ET molecules coordinated to the copper ions with the sulfur atoms of the ethylenedithio groups in all compounds. The Cu–S distances are found in the range 2.268(5)–2.417(8) Å, being close to the typical Cu^{I}–S coordination bond distances. Strong d–π interactions between d-electrons of the copper ions and π-electrons of the ET molecules can be expected through the Cu–S coordination bonds. ET molecules behave as *trans*-bidentate ligands bonding to two different copper ions in **1** and **3**, as *cis*-bidentate ligands in **2**, **5**, and **6**, and as monodentate ligands in **4**. In the crystal structure of **3**, there are two types of ET molecules in the crystal structure, where the first type is a *trans*-bidentate ligand and the second forms a stacking structure by itself. Compounds **1**, **2**, **4**, and **6** show semiconducting behavior down to low temperature ($\sigma_{RT} = 1.6 \times 10^{-2}$ S cm^{-1} and $E_a = 122$ meV for **1**, $\sigma_{RT} = 2.1$ S cm^{-1} and $E_a = 21$ meV for **2**, $\sigma_{RT} = 5.4 \times 10^{-4}$ S cm^{-1} and $E_a = 239$ meV for **4**, and $\sigma_{RT} = 5.1 \times 10^{-2}$ S cm^{-1} and $E_a = 207$ meV for **6**). On the other hand, in **3**, a metal-like region is observed along the *b*-axis and *c*-axis, due to the contribution of stacked ET molecules, and a metal–semiconductor transition occurs at 280 and 270 K, respectively. Also, **5** exhibits metallic conductivity in the temperature ranges 240–300 and 200–300 K along the *b*-axis and *c*-axis, respectively, despite the oxidation state of ET with 2+.

Introduction

In the past decade, the field of molecular-based functional materials has made significant progress, especially for bulk magnetic materials and highly conducting materials. As the next step, recently, the development of multifunctional molecular materials has attracted an increasing interest in the light of both applications to devices and fundamental science. In particular, materials combining conducting properties of π-conjugated organic radicals (π-electrons) with other physical phenomena, for example, magnetic interactions of transition metal complexes (d-electrons), are a subject of extensive studies. So far, two types of compounds of this kind have been synthesized and characterized, where the first type is a separated d$-\pi$ system (Figure 1a), and the second type is a fused d$-\pi$ system (Figure 1b) with π-conjugated molecules bonding to metal ions directly, for example, the $Cu(DMe\text{-}DCNQI)_2$ system.[1]

Many compounds of the first type have been reported, for example, the paramagnetic superconductor β''-$(ET)_4(H_2O)Fe^{III}(C_2O_4)_3(C_6H_5CN)$[2], the antiferromagnetic superconductor κ-$(BETS)_2Fe^{III}Br_4$[3] (BETS = bis(ethylenedithio)tetraselenafulvalene), and the ferromagnetic metal $(ET)_3[Mn^{II}Cr^{III}(C_2O_4)_3]$,[4] but compounds exhibiting interactions between

* To whom correspondence should be addressed. E-mail: yamashit@comp.metro-u.ac.jp.
[†] Tokyo Metropolitan University and CREST.
[‡] Nagoya University.
[§] University of Tokyo.

10.1021/ic0344362 CCC: $25.00
Published on Web 10/03/2003

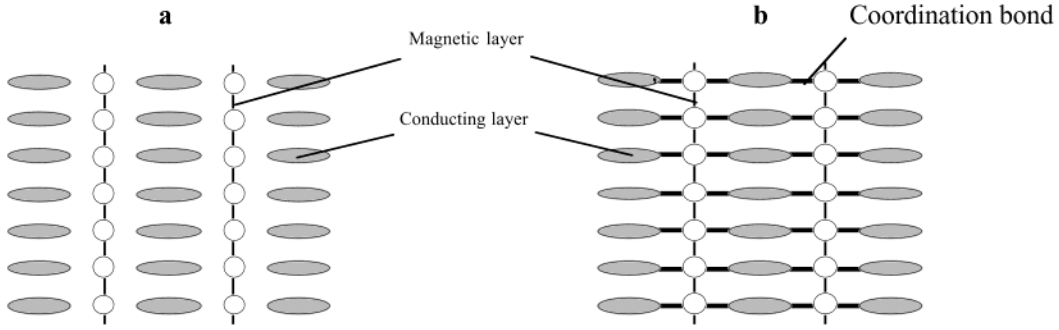

Figure 1. Separated d−π system (a) and fused d−π system (b).

conducting π-electrons and magnetic d-electrons, so-called d−π interactions, are limited[5] because the magnetic and conducting layer are absolutely separated from each other. On the other hand, so far few examples of the fused type are reported except for the $Cu(DCNQI)_2$ system.

Copper(II) halides readily oxidize TTF and its derivatives and provide a variety of charge-transfer complexes that have quite different structural and physical properties including metallic conductivity and superconductivity.[6] In the present study, the redox reactions between ET and $Cu^{II}Br_2$ were carried out, and new charge-transfer complexes $(ET)Cu^{I}_2Br_4$ (**1**), $(ET)_2Cu^{I}_6Br_9$ (**2**), $(ET)_2[Cu_4Br_6ET]$ (**3**), $(ET)_2Cu^{I}_2Br_4$ (**4**), $(ET)_2Cu^{I}_3Br_7(H_2O)$ (**5**), and $(ET)_2Cu^{I}_6Br_{10}$ (**6**) were obtained. X-ray crystal analyses of these compounds showed that ET molecules coordinated to copper ions with the sulfur atoms of the ethylenedithio groups in various coordination modes, such as monodentate, *trans*-bidentate, and *cis*-bidentate. These are limited examples of coordination bond formation between ET molecules and transition metal ions, which are fused d−π systems.[7]

A prototypical good example of fused types may be the $Cu(DMe\text{-}DCNQI)_2$ system that is electrically and magnetically active molecular compounds. In this system, Cu···N≡C coordination bond formations have been observed between copper ions and π-molecule DMe-DCNQI radicals, and 2-D sheets were constructed. It has been pointed out that the mixed valency of copper ion ($Cu^{1.3+}$) affords a d−π mixed metallic band. Moreover, a peculiar metal−insulator−metal re-entrant transition coupled with the appearance and disappearance of the magnetic ions (Cu^{II}) has been observed. In this system, however, the coexistence of the metallic π-conducting electrons and the localized magnetic moments could not be achieved. The magnetic moments of Cu^{II} appear only in the insulating state.

Compounds **1**−**6** are expected to be electrically active. We present herein these new fused type compounds and those physical properties.

Experimental Section

1. Syntheses. All chemicals used for the syntheses were of reagent grade quality. ET was purchased from Tokyo Kasei Kogyo Co., Ltd., and recrystallized from $CHCl_3$ before use. $Cu^{II}Br_2$ was purchased from Wako Pure Chemical Industries, Ltd., and used without further purification. THF and methanol were distilled from sodium/benzophenone and $MeOH/Mg(OMe)_2$, respectively. A redox reaction between ET and $Cu^{II}Br_2$ was carried out under such conditions that the Cu^{II} ion was always in excess throughout the course of reaction. Under nitrogen with exclusion of the light, after several weeks of diffusion, black crystals were obtained at room temperature. The detailed conditions are separately described in

(1) (a) Aumuller, A.; Erk, P.; Klebe, G.; Hunig, S.; Schutz, J. U.; Werener, H.-P. *Angew. Chem., Int. Ed. Engl.* **1986**, *25*, 740. (b) Kobayashi, A.; Kato, R.; Kobayashi, H.; Mori, T.; Inokuchi, H. *Solid State Commun.* **1987**, *64*, 45. (c) Kobayashi, H.; Miyamoto, A.; Kato, R.; Sakai, F.; Kobayashi, A.; Yamakita, Y.; Furukawa, Y.; Tasumi, M.; Watanabe, T. *Phys. Rev. B* **1993**, *45*, 3500. (d) Tomic, S.; Jerome, D.; Aumuller, A.; Erk, P.; Hunig, G.; Schutz, J. U. *J. Phys. C: Solid State Phys.* **1988**, *21*, L203. (e) Kobayashi, H.; Sawa, H.; Aomura, S.; Kato, R. *J. Am. Chem. Soc.* **1993**, *115*, 7870.

(2) Day, P.; Kurmoo, M.; Mallah, T.; Marsden, I. R.; Friend, R. H.; Pratt, F. L.; Hayes, W.; Casseau, D.; Gaultier, J.; Bravic, G.; Ducasse, L. *J. Am. Chem. Soc.* **1995**, *117*, 12209.

(3) Kobayashi, H.; Kobayashi, A.; Cassoux, P. *Chem. Soc. Rev.* **2000**, *29*, 325.

(4) Coronado, E.; Galan-Mascaros, J. R.; Gomez-Garcia C. J.; Laukhin, V. *Nature* **2000**, *408*, 447.

(5) (a) Enoki, T.; Yamaura, J.; Miyazaki, A. *Bull. Chem. Soc. Jpn.* **1997**, *70*, 2005. (b) Kobayashi, H.; Tomita, H.; Naito, T.; Kobayashi, A.; Sakai, F.; Watanabe, T.; Cassoux, P. *J. Am. Chem. Soc.* **1996**, *118*, 368. (c) Mori, T.; Fumiko, S.; Gunzi, S.; Inokuchi, H. *Chem. Lett.* **1987**, *5*, 927.

(6) (a) Urayama, H.; Yamochi, H.; Saito, G.; Sato, S.; Kawamoto, A.; Tanaka, J.; Mori, T.; Maruyama, Y.; Inokuchi, H. *Chem. Lett.* **1988**, 463. (b) Geiser, U.; Beno, M. A.; Kini, A. M.; Wang, H. H.; Schultz, A. J.; Gates, B. D.; Cariss, C. S.; Carlson, K. D.; Williams, J. M. *Synth. Met.* **1988**, *27*, A235. (c) Kini, A. M.; Geiser, U.; Wang, H. H.; Carlson, K. D.; Williams, J. M.; Kwok, W. K.; Vandervoort, K. G.; Thompson, J. E.; Stupka, D. L.; Jung, D.; Whangbo, M.-H. *Inorg. Chem.* **1990**, *29*, 2555. (d) Williams, J. M.; Kini, A. M.; Wang, H. H.; Carlson, K. D.; Geiser, U.; Montgomery, L. K.; Pyrka, G. J.; Watkins, D. M.; Kommers, J. M.; Boryschuk, S. J.; Crouch, A. V. S.; Kwok, W. K.; Schirber, J. E.; Overmyer, D. L.; Jung, D.; Whangbo, M.-H. *Inorg. Chem.* **1990**, *29*, 3272. (e) Kawamoto, A.; Tanaka, J.; Tanaka, M. *Acta Crystallogr., Sect. C* **1987**, *43*, 205. (f) Mori, T.; Sasaki, F.; Saito, G.; Inokuchi, H. *Chem. Lett.* **1987**, 927. (g) Geiser, U.; Wang, H. H.; Hammond, C, E.; Firestone, M. A.; Beno, M. A.; Carlson, K. D.; Nunez, L.; Williams, J. M. *Acta Crystallogr., Sect. C* **1987**, *43*, 656. (h) Kurmoo, M.; Talham, D. R.; Day, P.; Howard, J. A. K.; Stringer, A. M.; Obertelli, D. S.; Friend, R. H. *Synth. Met.* **1998**, *22*, 425. (i) Obertelli; Friend, R. H. *Synth. Met.* **1988**, *22*, 415. Kinoshita, N.; Takahashi, K.; Murata, K.; Tokumoto, M.; Anzai, H. *Solid State Commun.* **1988**, *67*, 465. (j) Lequan, M.; Lequan, R. M.; Mauno, G.; Delhaes, P. *J. Chem. Soc., Chem. Commun.* **1988**, 174. (k) Inoue, M. B.; Fernando, Q.; Inoue, M. *Synth. Met.* **1991**, *42*, 2069. (l) Kurmoo, M.; Kanazawa, D.; Day, P. *Synth. Met.* **1991**, *42*, 2123. (m) Inoue, M. B.; Inoue, M.; Fernando, Q.; Nebesny, K. W. *Inorg. Chem.* **1986**, *25*, 3976. (n) Inoue, M. B.; Cruz-Vazquez, C.; Inoue, M.; Pyrka, G. J.; Nebesny, K. W.; Fernando, Q. *Synth. Met.* **1988**, *22*, 231. (o) Inoue, M.; Inoue, M. B. *Rev. Inorg. Chem.* **1988**, *9*, 219.

(7) (a) Inoue, M. B.; Inoue, M.; Bruck, M. A.; Fernando, Q. *J. Chem. Soc., Chem. Commun.* **1992**, 515. (b) Ramos, J.; Yartsev, V. M.; Golhen, S.; Ouahab, L.; Delhaes, P. *J. Mater. Chem.* **1997**, *7* (8), 1313. (c) Kuroda-Sowa, T.; Hirata, M.; Munakata, M.; Maekawa, M. *Chem. Lett.* **1998**, 499. (d) Matsubayashi, G.; Yokoyama, K.; Tanaka, T. *J. Chem. Soc., Dalton Trans.* **1988**, 3059. (e) Tarutani, S.; Mori, T.; Mori, H.; Tanaka, S.; Takahashi, K. *Chem. Lett.* **1997**, 627.

the following paragraphs. The crystals were collected by filtration and separated under microscope.

(ET)Cu_2Br_4 (1). Diffusing crystallization between $Cu^{II}Br_2$ in methanol (9.0×10^{-2} M) and ET in THF (2.6×10^{-3} M) was carried out in a straight tube. After several weeks of diffusion, well-defined needle crystals were obtained. Anal. Calcd for (ET)Cu_2Br_4, $C_{10}H_8S_8Cu_2Br_4$: C, 14.45; H, 0.97. Found: C, 14.62; H, 1.04. IR(KBr): 891, 1041, 1174, 1272, 1313, 1400, 1411, 2077, 2914, 2966 cm^{-1}.

$(ET)_2Cu_6Br_{10}$ (2). Diffusing crystallization between 9.0×10^{-2} M $Cu^{II}Br_2$ in methanol and 2.6×10^{-3} M ET in TCE (trichloroethane) or DCE (dichloroethane) was carried out in a straight tube. After several weeks of diffusion, thin platelets were obtained. Because of a low yield of **2**, the elemental analysis was not carried out. IR(KBr): 1049, 1083, 1116, 1156, 1197, 1233, 1278, 1340, 1406, 1458, 1637, 2854, 2923 cm^{-1}.

$(ET)_2[Cu_4Br_6ET]$ (3). Diffusing crystallization between 1.1×10^{-2} M $Cu^{II}Br_2$ in methanol and 2.6×10^{-3} M ET in THF was carried out in a straight tube. After several weeks of diffusion, traces of platelet crystals were obtained. Because of a low yield of **3**, the elemental analysis was not carried out. IR(KBr): 1022, 1066, 1110, 1155, 1161, 1280, 1344, 1385, 1406, 1537, 1643, 2922 cm^{-1}.

$(ET)_2Cu_2Br_4$ (4). Diffusing crystallization between 1.1×10^{-2} M $Cu^{II}Br_2$ in methanol and 2.6×10^{-3} M ET in THF was carried out in a straight tube. After several weeks of diffusion, micro block crystals were obtained. Because of a low yield of **4**, the elemental analysis was not carried out. IR(KBr): 1022, 1041, 1073, 1091, 1124, 1153, 1284, 1346, 1398, 1446, 1633, 2852, 2923, 2958 cm^{-1}.

$(ET)_2Cu_3Br_7(H_2O)$ (5). Diffusing crystallization between 4.5×10^{-2} M $CuBr_2$ in methanol and 1.7×10^{-3} M ET in DCE was carried out in a straight tube. After several weeks of diffusion, platelet crystals were obtained. Anal. Calcd for $(ET)_2Cu_3Br_7(H_2O)$, $C_{20}H_{18}S_{16}Cu_3Br_7O$: C, 15.63; H, 1.18. Found: C, 15.64; H, 1.25. IR(KBr): 1280, 1344, 1390, 1629, 2919, 2968, 3433 cm^{-1}.

$(ET)_2Cu_6Br_{12}(H_2O)_2$ (6). Diffusing crystallization between 4.5×10^{-2} M $CuBr_2$ in methanol and 1.7×10^{-3} M ET in DCM (dichloromethane) was carried out in a straight tube. After several weeks of diffusion, platelet crystals were obtained. Because of a low yield of **6**, the elemental analysis was not carried out. IR(KBr): 1029, 1082, 1282, 1342, 1398, 1541, 1558, 1635, 2854, 2923, 3421 cm^{-1}.

2. X-ray Data Collections and Structural Determinations. Structural determinations of the single crystals of the products were conducted on a Rigaku RAXIS-RAPID imaging plate diffractometer utilizing graphite monochromated Mo Kα radiation ($\lambda = 0.71069$ Å) or Rigaku/MSC Mercury CCD with graphite monochromated Mo Kα radiation ($\lambda = 0.71070$ Å). The structures were solved by direct methods (SIR92)[8] and expanded using Fourier techniques.[9] The non-hydrogen atoms were refined anisotropically, while hydrogen atoms were introduced as fixed contributions. All calculations were performed using the teXsan crystallographic software package of Molecular Structure Corporation.[10]

2.1. The crystal structures of (ET)$Cu^{I}{}_2Br_4$ (**1**) have been refined in the monoclinic space group $P2_1/n$ (No. 14), the unit-cell parameters being $a = 9.401(7)$ Å, $b = 10.841(8)$ Å, $c = 10.035(8)$ Å, $\beta = 98.48(1)°$, $V = 1011.7(1)$ Å^3, $Z = 2$, and R_1 (R_w) = 0.055 (0.132).

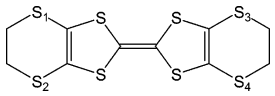

Figure 2. ET ligand.

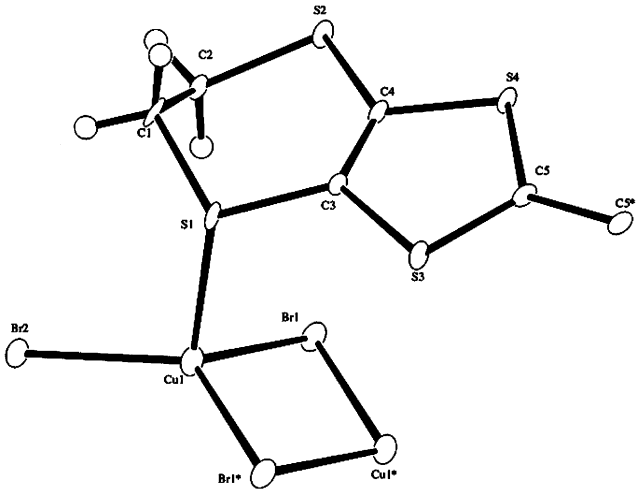

Figure 3. ORTEP drawing of a formula unit and neighboring bonding atoms of **1** with the atom numbering scheme (50% probability thermal ellipsoids).

2.2. The crystal structures of $(ET)_2Cu^{I}{}_6Br_{10}$ (**2**) have been refined in the monoclinic space group $P2_1$ (No. 4), the unit-cell parameters being $a = 14.708(4)$ Å, $b = 9.219(2)$ Å, $c = 17.087(5)$ Å, $\beta = 110.620(3)°$, $V = 2168(1)$ Å^3, $Z = 2$, R_1 (R_w) = 0.100 (0.244).

2.3. $(ET)_2[Cu_4Br_6ET]$ (**3**) crystallizes in the monoclinic space group $C2/c$ (No. 15) with the unit-cell dimensions $a = 53.06(1)$ Å, $b = 6.611(1)$ Å, $c = 15.030(3)$ Å, $\beta = 97.723(9)°$, $V = 5224.3(1)$ Å^3, $Z = 4$, R_1 (R_w) = 0.093 (0.190)

2.4. The crystal structures of $(ET)_2Cu^{I}{}_2Br_4$ (**4**) have been refined in the monoclinic space group $P2_1/c$ (No. 14), the unit-cell parameters being $a = 12.67(2)$ Å, $b = 7.407(9)$ Å, $c = 18.50(2)$ Å, $\beta = 92.75(2)°$, $V = 1733.7(3)$ Å^3, $Z = 4$, and R_1 (R_w) = 0.097 (0.230).

2.5. The crystal structures of $(ET)_2Cu^{I}{}_3Br_7(H_2O)$ (**5**) have been refined in the monoclinic space group $P\bar{1}$ (No. 2), the unit-cell parameters being $a = 8.215(3)$ Å, $b = 9.490(3)$ Å, $c = 14.602(6)$ Å, $\alpha = 104.65(1)°$, $\beta = 98.67(2)°$, $\gamma = 108.92(2)°$, $V = 1007.7(6)$ Å^3, $Z = 1$, and R_1 (R_w) = 0.093 (0.242).

2.6. The crystal structures of $(ET)_2Cu^{I}{}_6Br_{10}(H_2O)_2$ (**6**) have been refined in the orthorhombic space group *Pbcn* (No. 60), the unit-cell parameters being $a = 9.342(1)$ Å, $b = 15.558(2)$ Å, $c = 28.721(5)$ Å, $V = 4174(1)$ Å^3, $Z = 4$, and R_1 (R_w) = 0.096(0.231).

3. Physical Measurements. Because of the too small crystals, two-probe dc resistance measurements were conducted on single crystals using a Quantum Design PPMS. Measurement temperature was scanned in the range 2.0−315 K. Electrical contacts to the crystal were made with 15 μm gold wire and carbon paste. X-band electron spin resonance spectra (ESR) were recorded on polycrystalline sample at room temperature with a JEOL JEX-FE3X operating at 9.85 GHz and 1 mW. The reflectance spectra from 5000 to 6000 cm^{-1} were measured by use of the Olympus MMSP-RK microspectrophotometer. The spectra from 800 to 5000 cm^{-1} were measured with an infrared microspectrophotometer, JASCO MIR-300. For the measurements, single crystal surfaces were cleaned up to flat by tape. The absolute reflectivities were

(8) Altomare, A.; Burla, M. C.; Camalli, M.; Cascarano, M.; Giacovazzo, C.; Guagliardi, A.; Polidori, G. *J. Appl. Crystallogr.* **1994**, *435*, 27.
(9) Beurskens, P. T.; Admiraal, G.; Beurskens, G.; Bosman, W. P.; de Gelder, R.; Israel, R.; Smits, J. M. M. *The DIRDIF program system*; Technical Report of the Crystallography Laboratory; University of Nijmegen: Nijmegen, The Netherlands, 1994.
(10) *Crystal Structure Analysis Package*; Molecular Structure Corporation: The Woodlands, TX, 1985 and 1992.

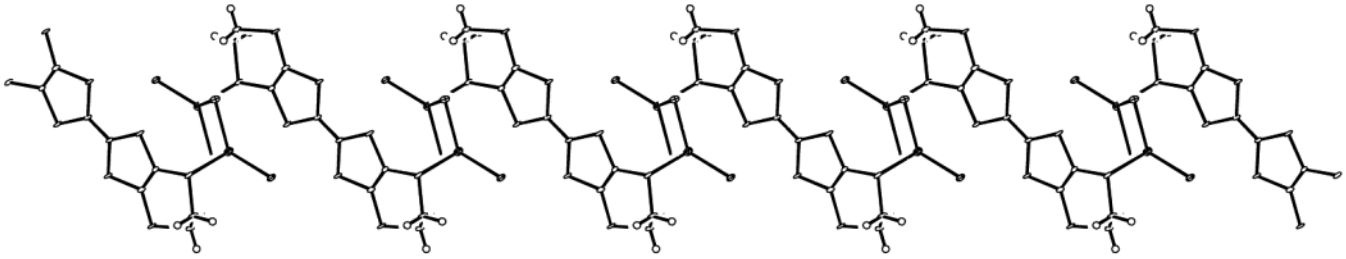

Figure 4. View of the one-dimensional chain $[-ET-(Br)Cu-(\mu_2\text{-}Br)_2-Cu(Br)-]_\infty$.

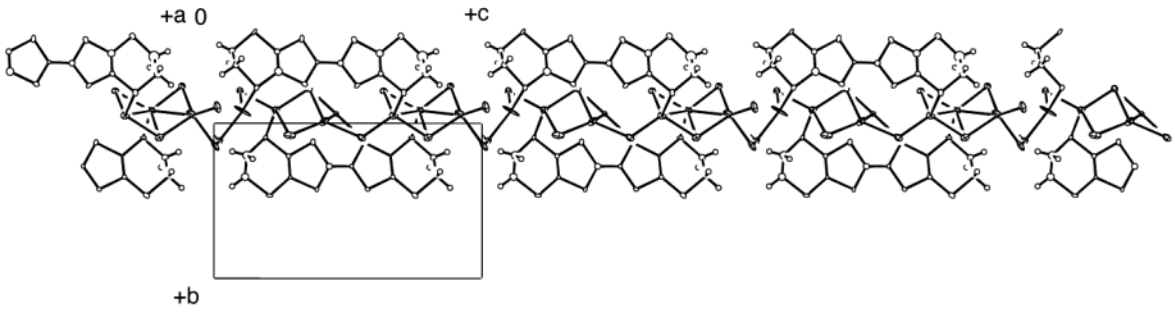

Figure 5. Crystal structure of **2**. The one-dimensional chain runs along the *c*-axis of the unit.

determined by using a silicon single crystal and an evaporated aluminum mirror as standard reflectors.

Results and Discussion

1. Crystal Structures. The most characteristic feature of the present compounds is the coordination bond formation between ET molecules and copper ions. These Cu−S coordination bonds are interpreted in the HSAB principle (hard and soft acids and bases principle). A sulfur atom of a thioether is classified as a soft base and Cu^I ion is classified as a soft acid. However, in the case of $Cu^{II}Cl_2$ used as acceptor, fused systems in which ET molecules coordinate to copper ions have not been obtained. The bromide ion that is a softer base than chloride ion is a key factor in the present study. The affinity between Cu^I ion and S atom of the ET molecule is enhanced by the bromide ions.

It was observed that the range of Cu−S distances is 2.268(5)−2.417(8) Å in these compounds, being close to the typical Cu−S coordination bond distances, 2.31−2.42 Å, reported for Cu^I complexes with thiourea and thioacetamide. The short distances suggest that Cu−S coordination bonds are formed. The present six compounds are classified into three groups according to the coordination modes of ET molecules: **4** is the group-I that has the ET monodentate ligand (S1 in Figure 2), **1** and **3** are group-II compounds that have ET *trans*-bidentate ligands (S1 and S4 in Figure 2), and **2**, **4**, and **6** are group-III compounds that have ET *cis*-bidentate ligands (S1 and S3 in Figure 2).

1.1. $(ET)Cu^I_2Br_4$ (1). An ORTEP representation of a formula unit of **1** is depicted in Figure 3. All the ET molecules coordinate to two copper ions with the two sulfur atoms in the *trans*-mode. The one-dimensional structure of copper complexes, $[-ET\text{-}(Br)Cu-(\mu_2\text{-}Br)_2-Cu(Br)-]_\infty$, running along the *c*-axis bridged by bromides and ET *trans*-bidentate ligands is shown in Figure 4.

The Cu−S distance is found to be 2.384(2) Å. All the copper ions are crystallographically equivalent and have the tetrahedral coordination geometries that are characteristic of the Cu^I species. Therefore, the copper ions are in the Cu^I state, and **1** is formulated as $(ET)^{2+}Cu^I_2Br_4$ according to the results of the elemental analysis. The central C(5)═C(5)[1] bond length is 1.43(1) Å, which shows that the charge on the ET molecule is 2+, which is consistent with this formula.[11] X-band ESR measurement at room temperature also confirmed the formula with no signals.

The interchain S···S contacts are found to be 3.270(3), 3.332(3), and 3.367(4) Å, which are much shorter than the sum of the van der Waals radii (3.70 Å).

1.2. $(ET)_2Cu^I_6Br_{10}$ (2). The crystal structure of **2** is shown in Figure 5. All the ET molecules coordinate to two copper ions with the two sulfur atoms in the *cis*-mode. The Cu−S distances are 2.298(8), 2.307(8), 2.375(8), and 2.417(8) Å.

One-dimensional copper complexes are running along the *c*-axis, as shown in Figure 5, that is capped by ET *cis*-bidentate ligands. Short intermolecular S···S contacts between ET molecules are not observed in the chain, but interchain S···S distances are found in the range 3.33−3.58 Å, much shorter than the sum of the van der Waals radii. This packing diagram projected along the *c*-axis of the unit cell, shown in Figure 6, suggests that **2** has a isotropic electronic structure in the *ab*-plane. This packing feature that forms mixed conducting layer resembles mixed *κ*-type packing structures[12] in ϵ-$(ET)_2(I_3)(I_8)_{0.5}$, ζ-$(ET)_2(I_3)(I_5)$, and $(ET)_2(I_3)(TlI_4)$, which are semiconductors.

1.3. $(ET)_2[Cu_4Br_6ET]$ (3). As shown in Figure 7, the crystal structure of **3** comprises two parts: the conducting ET layers and ET−copper one-dimensional chains. In the

(11) Abboud, K. A.; Clevenger, M. B.; de Oliveira, G. F.; Talham, D. R. *J. Chem. Soc., Chem. Commun.* **1993**, *20*, 1560. Chou, L. K.; Quijada, M. A.; Clevenger, M. B.; de Oliveira, G. F.; Abboud, K. A.; Tanner, D. B.; Talham, D. R. *Chem. Mater.* **1995**, *7*, 530.

(12) Beno, M. A.; Geiser, U.; Kostka, K. L.; Wang, H. H.; Webb, K. S.; Firestone, M. A.; Carlson, K. D.; Nunez, L.; Whangbo, M.-H.; Williams, J. K. *Inorg. Chem.* **1987**, *26*, 1913.

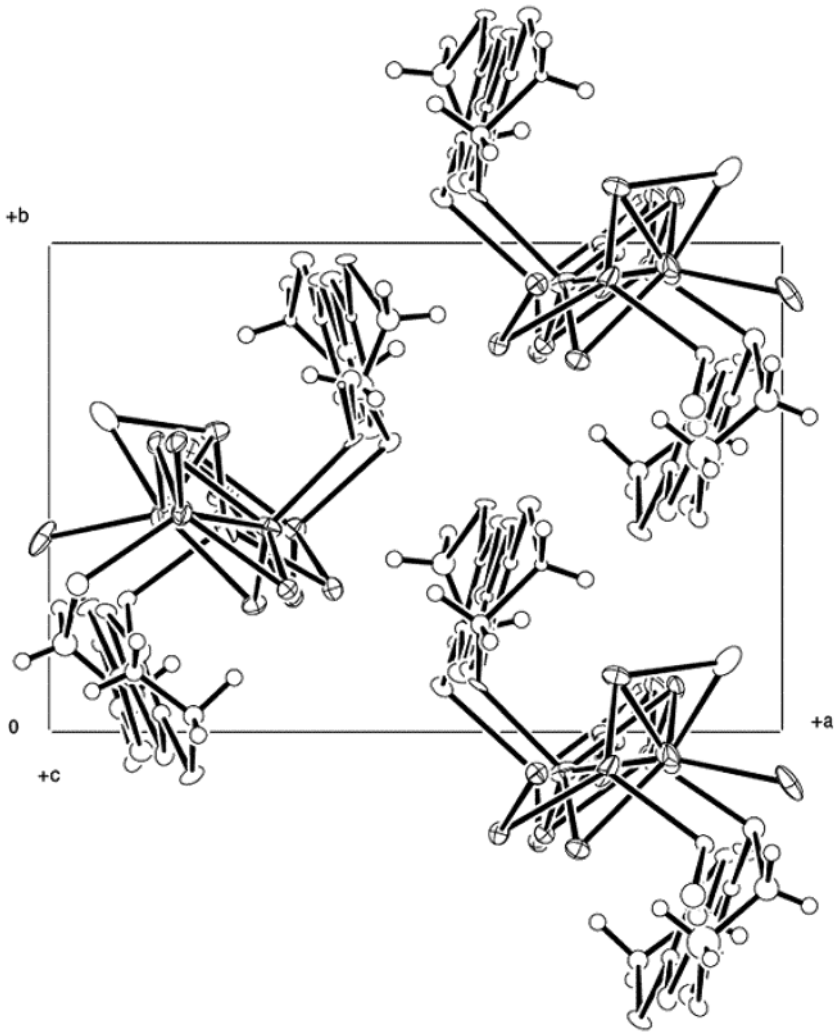

Figure 6. Packing diagram of **2** projected along the *c*-axis.

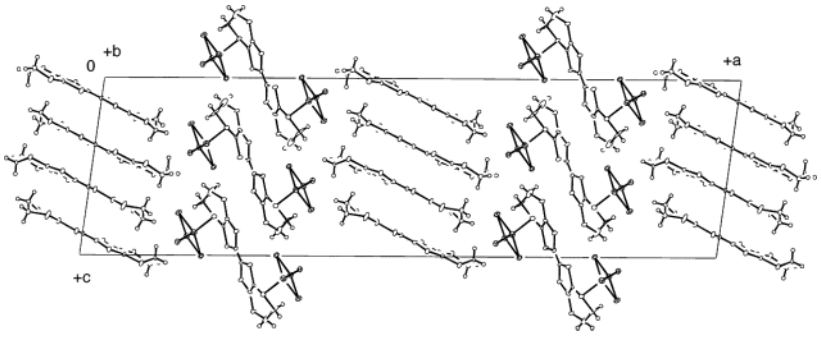

Figure 7. Packing diagram of **3** projected along the *b*-axis.

ET stacking layers, the ET molecules stack parallel to the *c*-axis, not coordinating to copper ions. In this layer, intermolecular S···S contacts are approximately found in the range 3.36−3.47 Å.

On the other hand in the ET-copper layers, the ET molecules coordinate to two copper ions with the two sulfurs in the *trans*-mode. The Cu−S distance is found to be 2.306-(3) Å. Two quasi-1D copper complexes, $[-Br-Cu(\mu_2-Br)_2-Cu-Br-]_\infty$, which are parallel to the *b*-axis, are bridged by ET molecules (B = trans-μ_2-ET) to form a ladderlike structure, as shown in Figure 8. In the chain, the Cu−Br distances are found in the range 2.35−2.54 Å.

An effective strategy for constructing conducting/magnetic hybrid materials is to combine organic conducting columns or layers and magnetic multidimensional lattices. But hybrid systems of such types are very limited.[4,13] Compound **3** is a hybrid material in which conducting layers and one-dimensional lattices coexist in crystal packing, structurally in such a category. But according to the coordination geometries, all the copper ions may be in monovalent states that are diamagnetic d^{10} states.

(13) Miyasaka, H.; Yoshino, Y.; Ishii, T.; Kanehama, R.; Manabe, T.; Yamashita, M.; Nishikawa, H.; Ikemoto, I.; Kishida, H.; Matsuzaki H.; Okamoto, H. *J. Solid State Chem.* **2002**, *168*, 418.

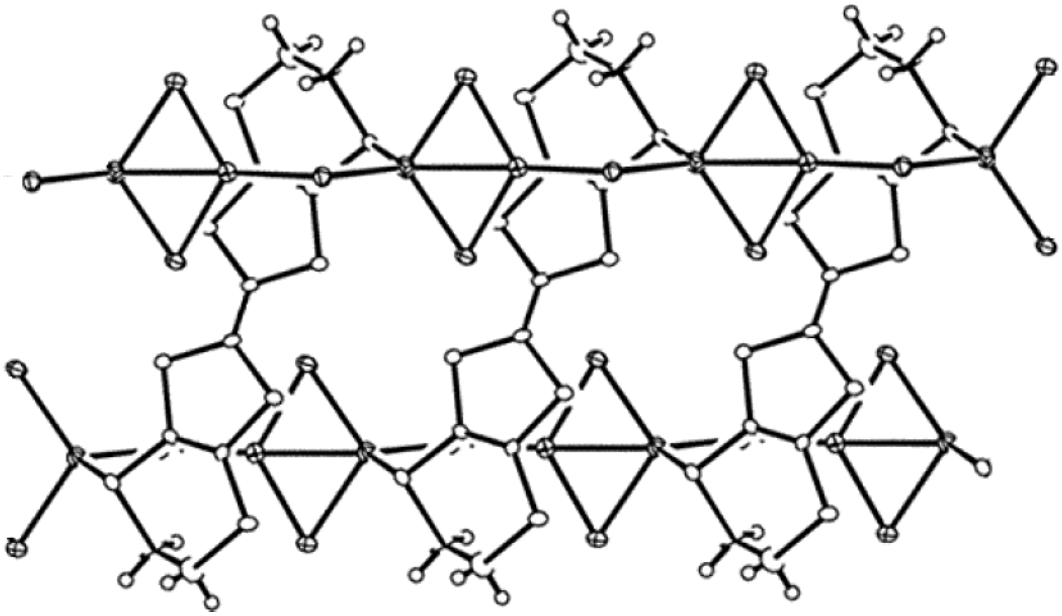

Figure 8. View of the ladderlike structure.

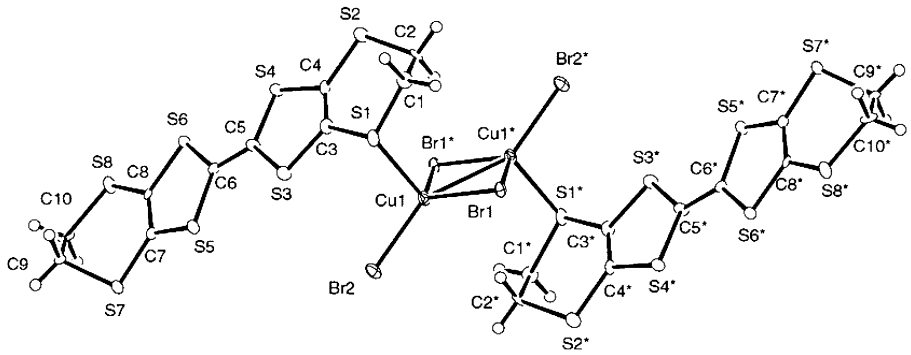

Figure 9. ORTEP diagram showing 40% thermal ellipsoids and atom labeling of **4**.

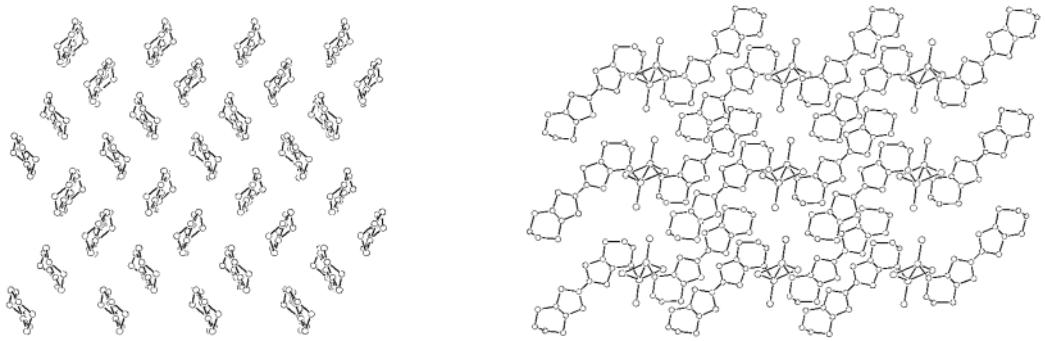

Figure 10. View of the κ-type conducting layer along the C═C bonds of ETs (left) and the alternating structure of **4** (right). H atoms have been removed for clarity.

1.4. $(ET)_2Cu^I_2Br_4$ (4). As shown in Figure 9, the ET molecule behaves as a monodentate ligand bonding to one copper ion with the S atom of the ethylenedithio group, forming a discrete ET_2Cu_2-dimer-dinuclear complex. The Cu−S distance is 2.370(4) Å. This is the first example of an ET monodentate ligand.

All the copper ions have tetrahedral coordination geometries that are characteristic of the Cu^I species, similar to **1**. Then, the formula of **4** is determined as $ET^+Cu^IBr_2$.

The Cu-dinuclear complexes exist discretely, but as shown in Figure 10, the ET ligands are packed in the κ-type arrangement.

In the ET-dimer there are no efficient S···S contacts shorter than 3.7 Å, but interdimer S···S distances are 3.27 and 3.27 Å, much shorter than the sum of the van der Waals radii. These are just the features of κ-types. The whole crystal structure of **4** consists of two phases: κ-type conducting layers and the bridging portions.

1.5. $(ET)_2Cu^I_3Br_7(H_2O)$ (5). The crystal structure of **5** is shown in Figure 11. ET molecules are expected to coordinate to two Cu ions with the two S atoms in the *cis*-mode, which is the same coordination mode as for **2**. But the population of Cu(1), Cu(2), Cu(3), Br(1), and the water molecule are not equal to 1.0. Then, it is obvious that not all the ET

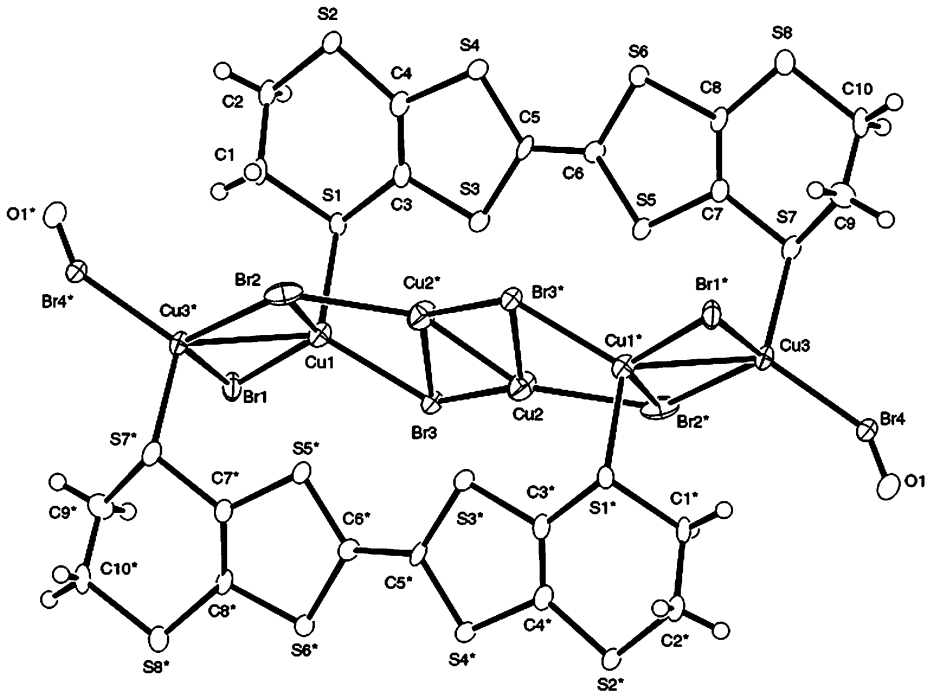

Figure 11. Structure of the discrete ET dimer of **5**.

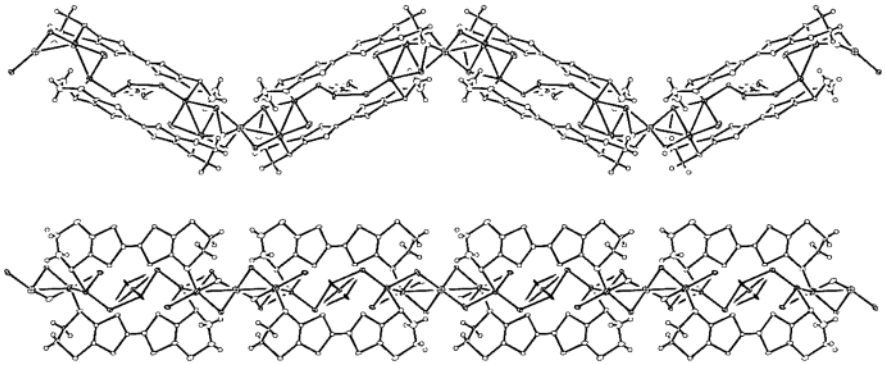

Figure 12. View of the zigzag one-dimensional chain of **6**, projected along the *b*-axis (top) and the *a*-axis (bottom).

molecules have *cis*-bidentate modes. The structure shown in Figure 11 is an averaged structure of the actual structure in the crystal.

X-band ESR measurement revealed that **5** had a closed electronic structure with no ESR signals. Therefore, the copper ions and ET molecules are in the Cu^{I} states and in the ET^{2+} states, respectively, and **5** is formulated as $(ET^{2+})_2Cu^{I}_3Br_7(H_2O)$. These discrete ET-dimer complexes are stacking along about the *a*-axis and form mixed conducting layers with the short S···S contacts: 3.27, 3.27, and 3.37 Å, respectively.

1.6. $(ET)_2Cu^{I}_6Br_{10}$ (6). Figure 12 shows the packing diagram of **6**, which is similar in **2** and **5**. ET molecules coordinate to two Cu ions with the two S atoms in the *cis*-mode. The crystal structure of **6** comprises fundamental ET-dimer units, connecting in a zigzag along the *c*-axis. The ET-dimer units are stacking in the *bc*-plane, forming mixed conducting, which is similar to that in **2**. In this layer, the intermolecular S···S contacts are found in the range 3.408(5)−3.549(5) Å, which are longer than those of **2**.

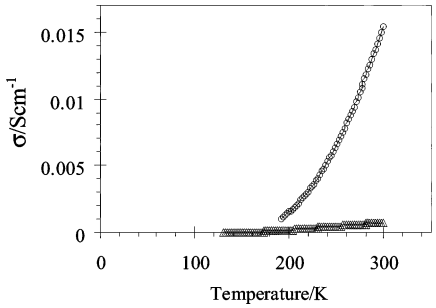

Figure 13. Temperature dependences of the conductivities of **1**, along the *c*-axis (○) and the perpendicular axis (△).

2. Conducting Properties. 2.1 $(ET)Cu^{I}_2Br_4$ (1). The electrical conductivity of a single crystal of **1** was measured in the temperature range 100−300 K as shown in Figure 13. Room temperature conductivities of **1** are 1.6×10^{-2} S cm^{-1} and 7.5×10^{-4} S cm^{-1} along the *c*-axis and the perpendicular direction, respectively, and activation energies are 122 and 105 meV, respectively. The crystal structure projected from the *c*-axis shows that **1** has an isotropic

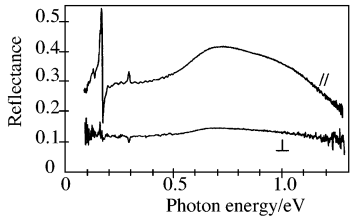

Figure 14. Polarized reflectance spectra of **1** measured on a single crystal directed parallel and perpendicular to the *c*-axis.

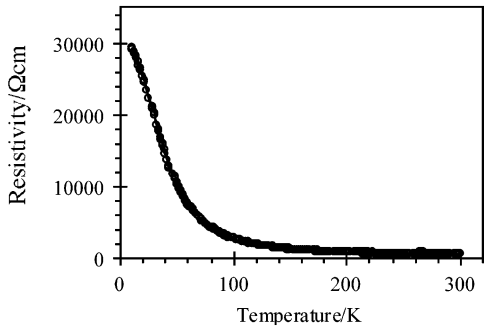

Figure 15. Temperature variation of resistivity for **2** along the *c*-axis.

structure in the *ab*-plane, and therefore, the electronic structure is also expected to be isotropic in this plane.

Figure 14 shows the room temperature reflectance spectra of single crystals of **1**. The spectrum polarized nearly parallel to the *c*-axis (∥*c*-axis) is typical of semiconductors in shape, consisting of a broad electronic absorption with a maximum at ca. 5800 cm^{-1} (0.7 eV), and corresponding to the charge-transfer between ET moieties.

The vibrational structure below 1400 cm^{-1} due to the A_g vibrations of ET (mainly C═C stretching) is activated by coupling with the electronic excitation. On the other hand, in the perpendicular polarization (⊥), the spectral shape is almost flat. This anisotropy is very consistent with the results of the resistivity measurements. The conducting pathway is running along the *c*-axis, that is, the direction of the one-dimensional chain.

These conducting data of **1** are inconsistent with the oxidation states of the ET molecules (ET^{2+}). It is possible that this high conductivity is attributable to impurities from the edges of the one-dimensional chains.

2.2. $(ET)_2Cu^I_6Br_{10}$ (2). The single crystal of **2** is very a thin plate film. Then, the electrical conductivity of **2** could be measured only along the *c*-axis, that is, the elongated crystal direction. Figure 15 shows the temperature dependence of the resistivity of **2**.

Between 300 and 10 K, **2** exhibits a semiconducting behavior with a small activation energy, $E_a = 21$ meV, and a room temperature conductivity, $\sigma_{RT} = 2.1$ S cm^{-1}, with no anomalies.

The polarized reflectance spectra of **2** measured over the spectral range 0.1−1.3 eV at room temperature are shown in Figure 16. Spectra of both polarizations are similar in shape, and prominent dispersions are found in the infrared region for both polarizations. This proves that **2** has metallic conduction electrons around room temperature and has a highly isotropic electronic structure within this plane (*bc*-plane). This reflectance spectra and the small activation energy show that **2** has a semimetallic electronic structure at room temperature.

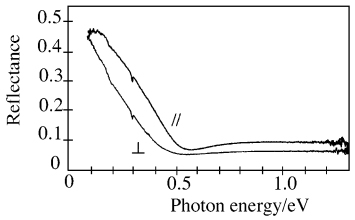

Figure 16. Polarized reflectance spectra of a single crystal of **2** at room temperature, with the polarizations nearly parallel and perpendicular to the *b*-axis.

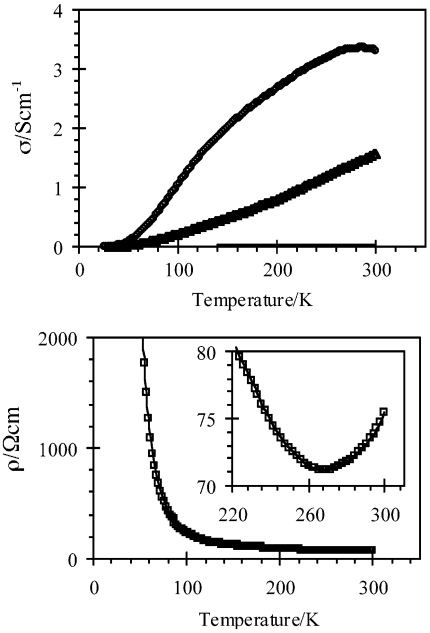

Figure 17. Comparison of the temperature dependences of conductivities of **3** along the *a*-axis (○), *b*-axis (△), and *c*-axis (□) (top) and temperature dependence of resistivity along the *c*-axis (bottom).

2.3. $(ET)_2[Cu_4Br_6ET]$ (3). The conductivity data for **3** are shown in Figure 17. A metallic regime is observed above 270 K along the *c*-axis, that is, the ET stacking direction, probably due to the ET conducting layer.

At about 270 K, an upturn in resistivity occurs, indicating the occurrence of a metal−semiconductor transition. Also, metallic behavior was also observed between 300 and 280 K along the *b*-axis. The room temperature conductivities and activation energies are 2.4 S cm^{-1} and 22 meV, 3.3 S cm^{-1} and 22 meV, and 2.5×10^{-2} S cm^{-1} and 17 meV along the *a*-, *b*- and *c*-axis, respectively.

2.4. $(ET)_2Cu^I_2Br_4$ (4). The electrical conductivity of a single crystal of **4** was measured in the temperature range 100−300 K, as shown in Figure 18. Because of the micro block crystal morphology, the anisotropy of conductivity is under investigation now. It conforms to the classical activation behavior of a semiconductor. The room temperature conductivity of **4** is 5.4×10^{-4} S cm^{-1}, and the activation energy is 239 meV with no anomalies.

2.5. $(ET)_2Cu^I_3Br_7(H_2O)$ (5). The temperature dependence of resistivities of **5** is shown in Figure 19. This compound

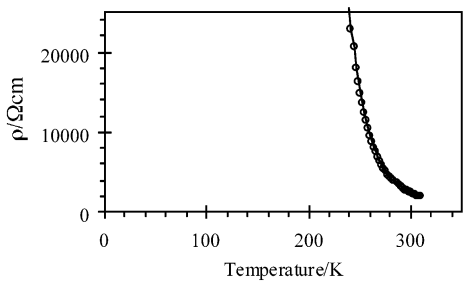

Figure 18. Temperature dependence of resistivity of **4**.

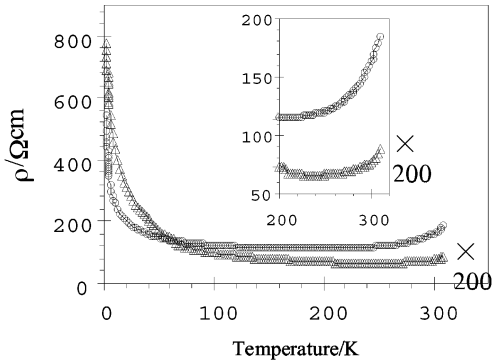

Figure 19. Temperature dependences of the resistivities of **5** along the *b*-axis (○) and *c*-axis (△).

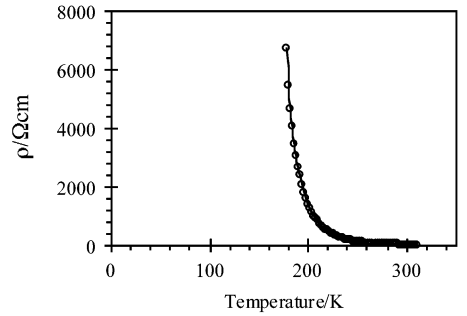

Figure 20. Temperature dependence of resistivity of **6**.

behaves as a metal down to 240 and 200 K along the *b*-axis and *c*-axis, respectively. The room temperature conductivities are 2.3 S cm^{-1} and 5.4 × 10^{-3} S cm^{-1}, respectively.

This high conductivity and metallic behavior of **5** are inconsistent with the electronic structure (ET^{2+} and Cu^{I}). It is assumed that the high conductivity is attributable to construction of the conducting layer and formation of the Cu−S coordination bond. We propose the presence of conducting carriers derived from the Cu−S coordination bonds, which are back-donations from copper ions to ET molecules.

2.6. $(ET)_3Cu^{I}_6Br_{10}(H_2O)_2$ (6). The electrical conductivity of a single crystal of **6** was measured in the temperature range 100−300 K as shown in Figure 20. Throughout the whole temperature range of measurement, **6** exhibits semiconducting behavior with a room temperature conductivity 5.1 × 10^{-2} S cm^{-1} and an activation energy 207 meV. However, the anisotropy of conductivity is under investigation now. Higher conductivity is expected along the conducting layer, similar in **2**.

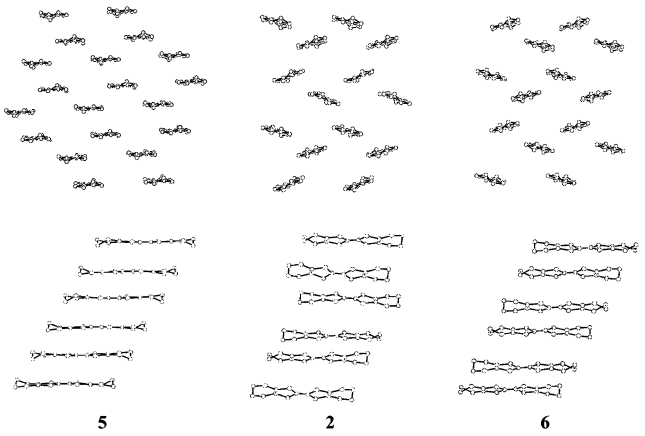

Figure 21.

The mixed conducting layers are constructed from ET molecules and the bridging copper complexes in **2**, **5**, and **6**. Figure 21 shows the packing features of **2**, **5**, and **6** projected along the ET long axis. The packing structures of **2** and **6** are isostructural except for the S···S distances. In contrast, that of **5** is slightly different in the conducting layer. In all these layers, efficient S···S contacts are observed.

Conclusion

New charge-transfer salts $(ET)Cu_2Br_4$ (**1**), $(ET)_2Cu_6Br_{10}$ (**2**), $(ET)_2[Cu_4Br_6ET]$ (**3**), $(ET)_2Cu_2Br_4$ (**4**), $(ET)_2Cu_3Br_7(H_2O)$ (**5**), and $(ET)_2Cu_6Br_{10}$ (**6**) were obtained by slowly diffusing $Cu^{II}Br_2$ and ET. The present compounds are limited examples of fused systems in which ET molecules directly coordinate to copper ions. It is revealed that these compounds are diamagnetic but highly conducting materials. In particular, **5** exhibits metallic behavior in the high temperature region despite the oxidation states of ET molecules (ET^{2+}). A further synthetic challenge will be the development of the d−π system by doping magnetic moments into the copper sites, for example Cu^{II} ions or other magnetic transition metal ions. Our efforts are continuing in this direction.

Acknowledgment. This work was partly supported by a Grant-in-Aid for Science Research ("Metal-Assembled Complexes") from the Ministry of Education, Culture, Sports, Science and Technology, Japan (M.Y.) and Kumagai Science Foundation (H.M.).

Supporting Information Available: X-ray crystallographic data (CIF files), including a table of the atomic coordination, bond angles, and bond lengths. This material is available free of charge via the Internet at http://pubs.acs.org.

IC0344362